Article

Not peer-reviewed version

Physically and Chemically Activated Carbon from Coffee Waste in High Performance Supercapacitor Electrodes

Sami Mukhiemer , Allan Daraghmeh * , Heba Nassar , Shahzad Hussain , Hanyi Lim , Hyobin Han , Tae Woo Kim , Hikmat Said Hilal *

Posted Date: 11 October 2024

doi: 10.20944/preprints202410.0924.v1

Keywords: Waste coffee; Activated carbon; Physical activation; Physical-chemical activation; Supercapacitor electrode

 doi:10.20944/preprints202410.0924.v1

Article

Physically and Chemically Activated Carbon from Coffee Waste in High Performance Supercapacitor Electrodes

Sami Mukhiemer [1], Allan Daraghmah [1,*], Heba Nassar [2], Shahzad Hussain [3], Hanyi Lim [4], Hyobin Han [4], Tae Woo Kim [4] and Hikmat S. Hilal [2,*]

[1] Department of Physics, An-Najah National University, Nablus, P400, Palestine
[2] Department of Chemistry, An-Najah National University, Nablus, P400, Palestine
[3] Department of Engineering, University of Cambridge, Trumpington St. CB2 1PZ, UK
[4] Hydrogen Research Department, Korea Institute of Energy Research, 152, Gajeong-ro, Yuseong-gu, Daejeon 34129, Republic of Korea
* Correspondence: allan.d@najah.edu (A.D.); hshilal@najah.edu (H.S.H.)

Abstract: Biowaste sources, like coffee wastes (CWs), are considered for advanced materials. CW was assessed to prepare activated carbon for supercapacitor electrodes, but showed low performance compared to other counterparts. Enhanced CW activation process may help address this limitation. In this study, CW was subjected to two activation methods: physical (pyrolysis) activation and physical-chemical activation using $ZnCl_2$, to determine the more effective approach. Both resulting materials were analyzed using SEM, TEM, BET, Raman spectroscopy and XRD. The physical-chemical activation yielded activated carbon with better characteristics, including a higher specific-surface area (SSA) of ~830 m^2/g, compared to 458 m^2/g from the physical activation. With its promising potential for supercapacitor electrodes, the former activated carbon was singled out for supercapacitor study. Cyclic voltammetry revealed a specific capacitance of 261 F g^{-1}, and energy density of 18.3 Wh/kg, with power density of 360 W/kg at a current density 0.33 A/g. Charge-discharge studies showed a specific capacitance of 150 F g^{-1} at the same current density. Electrochemical impedance spectroscopy indicated a specific capacitance of 180 F g^{-1}, with an equivalent series resistance of 0.56 Ω at a low frequency of 0.01 Hz. The electrode exhibited exceptional characteristics, maintaining high stability over 5,000 charge-discharge cycles.

Keywords: waste coffee; activated carbon; physical activation; physical-chemical activation; supercapacitor electrode

1. Introduction

Many reasons stand behind considering bio wastes as sources for carbon materials in modern devices. Firstly, recycling bio wastes prevents the widespread environmental contamination from random dumping. Secondly, the produced carbon is useful as a low cost and safe material in electronic devices. Thirdly, the strategy minimizes dependence on the hazardous fossil sources [1-3]. A promising application area is supercapacitor (SC) technology for energy storage. The SC is a device with two high specific surface area (SSA) electrodes, a separator and an electrolyte solution. Compared to conventional capacitors, SCs have much higher capacitance [4-7]. With potentially high power yields, SCs are considered in various electronic devices, and specifically electric cars, competitively with batteries [5, 8].

The Ragone plots, describe how SCs are at intermediary position between batteries and conventional capacitors[9]. The plots combine energy density and power density output values for various energy storage devices, including fuel cells, batteries, SCs together with conventional capacitors. For a given device, lowering the equivalent series resistance increases the energy density, while raising the voltage window increases the power density [10-12].

 doi:10.20944/preprints202410.0924.v1

The need for higher-energy density storage devices continuously increases to meet expanding demands for modern electronic devices. As in batteries, electrochemical capacitors (ECs) attract special attention by virtue of their high storage density, low-temperature performance and multiple charge-discharge cycles. Unlike batteries and fuel cells, SCs involve no real chemical reactions, and function for prolonged life cycles [13], which is one virtue. SCs with both high energy density (like batteries) and high-power density (like capacitors) at the same time, are highly needed. SC research is thus active to achieve this feature.

In SCs, very high specific surface area (SSA) electrodes, with high conductivity, are used. The need for carbon materials in SCs is thus justified. Activated carbons (ACs) are conducting materials, thermally and chemically stable, and can have large SSAs with high micropore volumes. With high adsorption capacity and tunable pore structures [14], ACs are being considered in various energy-storage devices such supercapacitors [15, 16].

AC characteristics (surface, pore structure and adsorption capacity) are affected by preparation and activation methods. Two types of activation are widely known, physical activation and chemical activation. In chemical activation, impregnation with a suitable material is used. Examples of widely used chemical activating agents are: KOH, NaOH, K_2CO_3, $ZnCl_2$ or H_3PO_4. The activating agents, which are used in combination with mild physical processing, ensure pyrolytic decomposition of the precursor material at lower processing temperature, with less tar formation [17, 18]. In physical activation, the precursor material is partially gasified under inert atmosphere at a high temperature, and then activated with oxidizing gasses such as steam, air, carbon dioxide or mixed gases [18].

Chemical activation is a simple process, and is advantageous in terms of processing time, low temperature and high yield with high porosity. However, physical activation is still preferable at commercial scale, due to higher control on characteristics and simplicity [19].

High temperature pyrolysis can be coupled with poro-genic processes, using NaOH or KOH activation. Hazelnut shell hydrothermal carbonization (HTC) was studied by three various poro-genic methods namely simple-heat treatment, KOH activation and MgO templating. Better electrochemical characteristics (with higher SSA and effective micro-porosity) were reported in anode materials for energy storage [19, 20]. Chestnut shell based ACs, activated by KOH, were reported by Jiang et al. [21]. Effect of pre-carbonized stuff and KOH ratio was studied. SSA values of 1829.7 $m^2\ g^{-1}$ were observed for samples activated with biochar to KOH at 1 to 3 ratios. The AC showed highest capacitance of 238.2 Fg^{-1}. KOH was also used as activating agent at 600–900 ºC for 2 h, and yielded N-doped AC with a large SSA 3401 $m^2\ g^{-1}$ and a high specific capacitance 346 F g^{-1}. The energy density was 22.4 W h kg^{-1} at 0.5 A g^{-1} with high capacity stability (97.6% after 5000 cycles at 1 A g^{-1}) [22]

Chesnut shell-based AC, activated with $ZnCl_2$, exhibited SSA of up to 1987 $m^2\ g^{-1}$ with a specific capacitance105.4 F g^{-1} [23]. Hong et al. used K_2SO_4 to activate chestnut shell-based AC and reported an SSA 1412 $m^2\ g^{-1}$ with a specific capacitance 265 F g^{-1}, but with only a low current density of 0.1 A g^{-1}[22].

$KHCO_3$ was described to activate AC, from chestnut shells, for supercapacitor electrodes [22]. Biochar activation with $KHCO_3$ yielded porous carbons with high SSA 2298 $m^2\ g^{-1}$ and specific capacitance 387 F g^{-1} (at 2 A g^{-1}) with high stability 98.68% after 10,000 charge-discharge cycles at 30 A g^{-1} [22, 24]. N-doped porous carbon from edible Chinese water chestnut corms, was also reported [23].

Melamine also activated chestnut shell-based carbons [24]. The AC exhibited a current density 0.5 A g^{-1}, specific capacitance 402.8 F g^{-1} and SSA 691.8 $m^2\ g^{-1}$.

Depending on their regional agricultural resources and biowastes, researchers tend to focus their study attention. For this reason, in many regions people make their studies on chestnut, hazelnuts and others.

Other sources are globally spread, such as coffee wastes (CWs), since coffee is widely used in many places. It is reported that in early 2020s, more than 5 million tons of coffee was globally consumed [25]. More recently, the amounts of CW were reported to exceed 8 million tons [26]. ACs,

 doi:10.20944/preprints202410.0924.v1

with high surface areas and pore volumes from CW, were widely prepared and used for adsorption of various materials [25, 27-29].

CWs thus deserve to be studied. Few reports were published on CWs in supercapacitors. A flexible supercapacitor with a specific capacitance value of 139 F g^{-1} at 0.5 A g^{-1}, a specific energy 12.5 W h kg^{-1} and a specific power of 202 W kg^{-1}, was prepared from nitrogen 8%-doped AC. The supercapacitor functioned for more than 5,000 cycles with ~90% retained capacitance [30]. Chiu et al prepared AC in one combined process (physical and chemical activations) with various activating agents and found KOH as best choice to reach a specific capacitance 105.3 F g^{-1} [31]. M Biegun, et.al, used the hydrothermal acidic hydrolysis, then the KOH activation, at 800 ºC, to activate coffee waste, and obtained a high specific surface area of ~2900 m^2 g^{-1}. Using a liquid ionic electrolyte, the observed specific capacitance was 178 F g^{-1} at 20 ºC and 50 A g^{-1} [32]. Omkar Khadka et al. recently prepared supercapacitor electrodes from coffee wastes, first by chemical activation with $ZnCl_2$ 1:1 ratio, then by physical activation at 700 ºC, and observed a specific capacitance of 113.8 F g^{-1} at 1 A g^{-1} [33]. In a recent review, Davidraj et al reported the possibility of food waste materials to produce electrodes for energy storage devices [34]. The report listed a number of papers using CWs in supercapacitor electrodes. In another more recent review, Pagett et al reported on CWs in supercapacitor electrodes [26]. With the exception of one 2008 report that showed high specific capacitance [35], more recent papers showed specific capacitance values of only less than 160 F g^{-1} [26].

From literature, it can be noted that the AC prepared from coffee wastes showed lower performance than other ACs prepared from other sources such as chestnuts and hazelnuts. Moreover, the study on the coffee based ACs was not comprehensive, as it did not include important characteristics such as surface area or pore size that critically affects the electrode performance.

As CW is a promising source of AC, more study is needed to increase the CW based supercapacitor performance. The present study will assess the added value of using a chemical activating agent to the physical activation of CWs. Instead of using the highly corrosive KOH activating agent, reported earlier, the environmentally friendly and low cost $ZnCl_2$ is used here. The choice for $ZnCl_2$ is based on its acidic nature and efficiency as described in earlier reports where it yielded ACs with high surface areas [36]. $ZnCl_2$ was described in activating coffee waste for supercapacitor electrodes where specific capacitance was 134 F g^{-1} at 1 A g^{-1} using organic solvents, with equivalent series resistance more than 20 Ω [37]. Effect of activation method on various AC characteristics, such as specific surface areas, pore sizes and morphology, will be studied. The activating agent should chemically drill pores through the carbon matrix and increase its porosity. Various methods, such as XRD, SEM, BET and Raman spectra, will be used to test this effect. The AC suitability for supercapacitor electrodes, will be assessed, taking into consideration specific capacitance, power density and stability. The goal is to produce supercapacitor, with stable, porous and high surface area electrodes, from coffee-waste based AC, with and higher performance (in terms of specific capacitance and power output) than those described in literature. The basic assumption is that these features are achievable by adding a suitable chemical activating agent during CW pyrolysis. With a targeted specific capacitance value above 250 F g^{-1}, the results observed here were not precedented to our knowledge.

2. Materials and Methods

2.2. Starting Materials

Organic solvents, such as acetone, acids and bases, were purchased Sigma-Aldrich in pure forms. Coffee wastes was taken from freshly used Turkish coffee drinks (*Arabica* type). The coffee was processed according to Turkish coffee drink protocols, with fine grinding, and boiled. The CW was isolated and stored in a refrigerator for processing. The glass fiber separator (-M 5V5) has been purchased from Alter-Lab.

 doi:10.20944/preprints202410.0924.v1

2.2. Equipment

A hydraulic press (Shimadzu), equipped with pressure gauge, was used to make AC disks. The sample was pressed at 7 tons. The value was based on earlier recommendation [36].

A standard Teflon Swagelok cell, with 10 mm in diameter with stainless steel electrodes, was used for supercapacitor testing. The cell was connected to the potentiostat/Galvanostat (VoltaLabPGZ402). The working electrode was connected to one side, while the counter and the reference electrodes were connected together. The internal reference cell was used as reference. The VoltaMaster 4 software, was used for electrochemical measurements. AC morphology and surface structure were examined by scanning electron microscopy (SEM) (Hitachi- S-4800) on a Field-Emission machine. Transmission Electron Microscopy (TEM) was measured on a JEM-ARM200F system. Brunauer-Emmett-Teller (BET) was measured on a Micromeritics-3Flex 3500 equipment. X-Ray diffraction was measured on A PAN-alytical X'Pert-PRO X-Ray diffraction equipment, using a Cu Kα as a source. X-ray photoelectron spectroscopy was measured on a Thermo Scientific machine model K-alpha+. Raman spectra were measured on an OlympusBX41M equipment. SEM, XRD, TEM, BET, XPS and Raman spectra were all measured in the labs of the KIER, Daejeon, Korea.

2.3. AC Preparation

The CW material was activated by two methods, namely the physical and the chemical activation.

- ***Physical activation (AC_{Phys})***

Pre-dried *Arabic* coffee waste (100 g) was rinsed with hot distilled water (400 mL), then with cold distilled water (400 mL), and finally rinsed with ethanol. This was to remove soluble coffee ingredients. The remaining solid waste was left to dry at room temperature for 24 h, then heated in an oven at 70 ºC for 12 h. The waste was then heated at 800 ºC for 2 h under nitrogen atmosphere. The resulting AC_{Phys} was stored in a desiccator for further use. The net mass for the AC_{Phys} was 75.3 g.

- ***Chemical-physical activation ($AC_{Phys\text{-}Chem}$)***

Pre-dried *Arabica* coffee waste (100 g) was washed with hot distilled water (400 mL) and then with cold distilled water (400 mL), and finally rinsed with ethanol. The coffee waste was left to dry at room temperature for 24 h, then heated in an oven at 70 ºC for 12 h. The waste was then magnetically stirred with $ZnCl_2$(s) (in a 1:1 mass ratio) at 60 ºC for 24 h. The solid was dried at room temperature for 24 h and then in an oven at 70 ºC for 7 h. The solid was heated at 800 ºC for 2 h. The resulting $AC_{Phys\text{-}Chem}$ was cooled and stored in a desiccator for further use. The net mass for $AC_{Phys\text{-}Chem}$ was 47.6 g.

2.4. AC Disc Electrode Preparation

A sample of activated carbon was ball milled to fine powder with Agat mortar for 10 min. The AC was mixed with PVDF polymer in a 93:7% ratio, and was magnetically stirred with acetone (15 mL). The mixture container was then sonicated in a bath at 35 ºC for 20 min. The solid was separated and dried in an oven at 70 ºC for 2 h. The AC powder (0.03 g) was then used to make electrode discs, which were pressed in a mold under hydraulic pressure of 7 tons. The AC disc diameter was 10 mm and the disc thickness was ~0.19 mm.

2.5. Electrochemical Methods

Electrochemical characteristics of activated carbon were analyzed by using various methods, namely cyclic voltammetry (CV), galvanostatic charge-discharge (GCD) and electrochemical impedance spectroscopy (EIS). A Swagelok cell was used in electrochemical studies. One disc was loaded as a coating layer on one stainless steel electrode. A fiberglass disk separator (with diameter of 10 mm) was immersed in KOH electrolytic solution (6 M) for 5 min. The immersed fiberglass separator was then carefully taken by tongs and firmly stacked on the AC electrode, as a coating. The

 doi:10.20944/preprints202410.0924.v1

other AC disc was stacked onto the separator. Then the cell was then firmly assembled to prevent gaps and bubbles between electrodes, and to disallow any cell component movements. The assembled Sawgelok cell was connected to the PGZ 402 Potentiostat/Galvanostat, using the 2-terminal mode. The voltaMaster 4 software was utilized in data collections. The CV measurements were performed for each electrode by scanning the potential from 0.0 to 1.0 V at different scan rates

The GCD study was performed at various current densities. The current density was switched between positive and negative values, for charging and discharging, respectively. The results were acquired and analyzed using Origin software.

3. Results

- ***AC disc characterization AC Morphology***

Figure 1 shows SEM micrographs for both AC material in pressed disc forms. The AC_{Phys} and $AC_{Phys\text{-}Chem}$ materials exhibited different surface morphologies. The $AC_{Phys\text{-}Chem}$ is more porous than the AC_{Phys}. This is due to the chemical activation which further affects the AC surface, in addition to physical activation, as reported earlier [38, 39]. As stated above, the acidic $ZnCl_2$ activating agent interacts with the carbon matrix and makes it more porous.

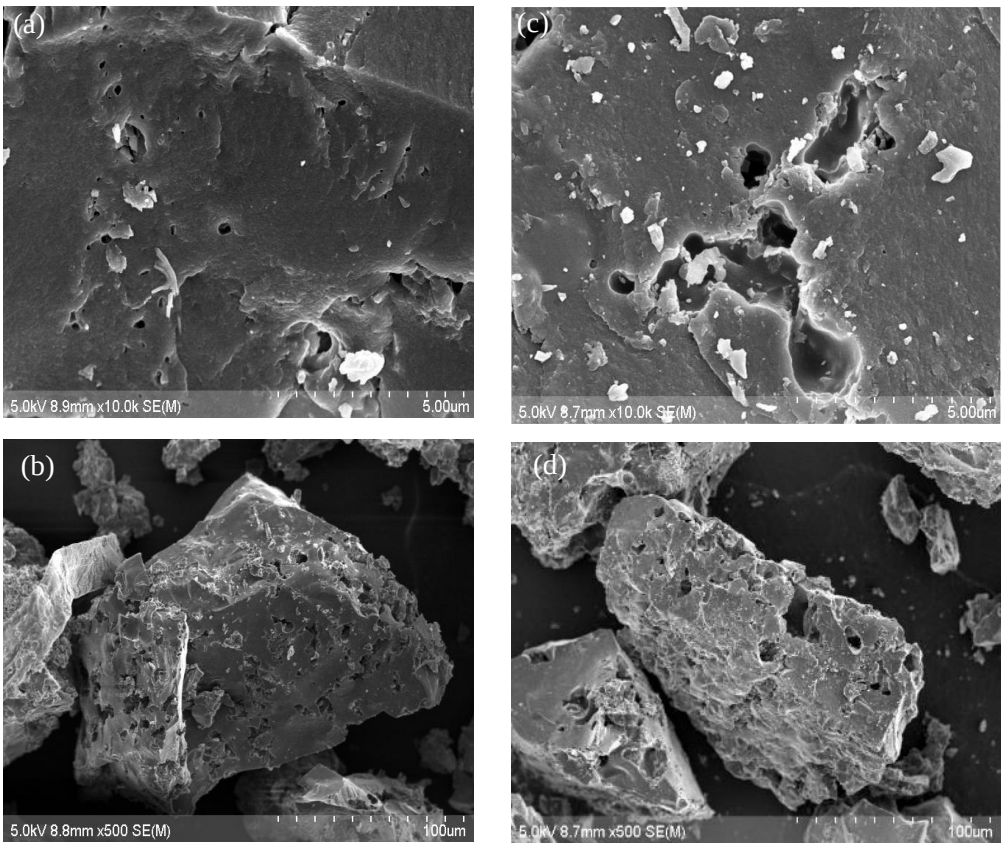

Figure 1. SEM micrographs measured for coffee waste based ACs in as pressed discs. (a) and (b) for AC_{Phys}; (c) and (d) for $AC_{Phys\text{-}Chem}$.

In Figure 2, TEM micrographs for both AC materials are shown. In each case, white dots can be observed indicating pores. The $AC_{Phys\text{-}Chem}$ was more porous, with higher homogeneity, than AC_{Phys}.

Preprints.org (www.preprints.org) | NOT PEER-REVIEWED | Posted: 11 October 2024 doi:10.20944/preprints202410.0924.v1

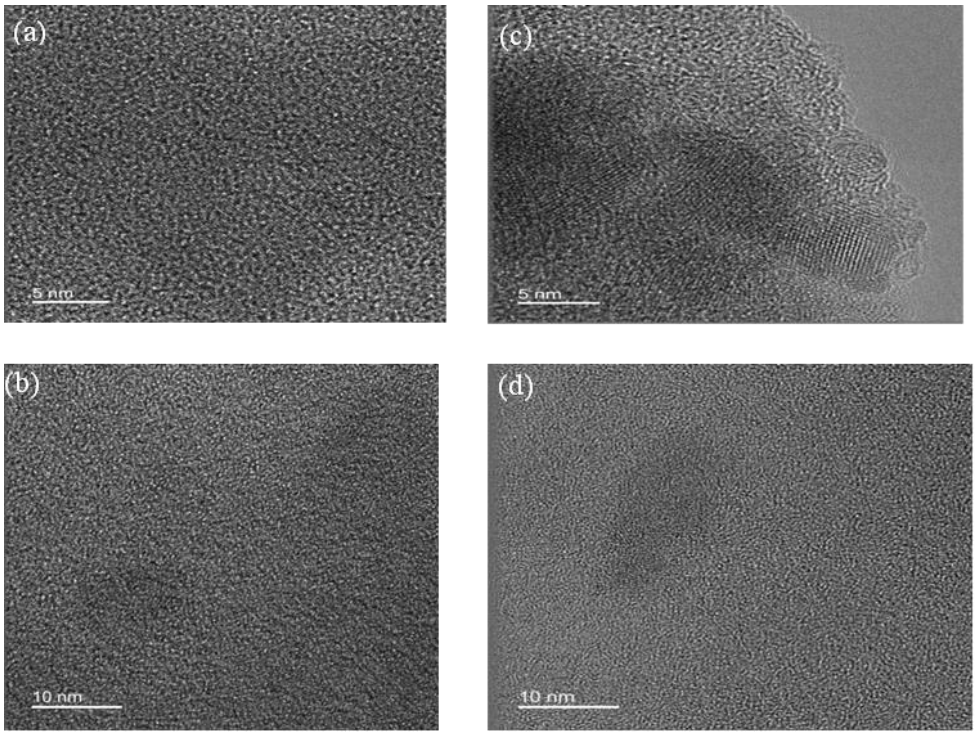

Figure 2. TEM micrographs measured coffee waste based ACs as pressed discs. (a) and (b) for AC_{Phys}; (c) and (d) for $AC_{Phys\text{-}Chem}$.

- *AC porosity*

Porosity for the two AC materials was measured using the BET method. Porosity involves specific surface area (SSA), por size distribution (PSD) and total specific pore volume. Adsorption/desorption isotherms were measured for both AC materials in pressed disc forms. Figure 3 summarizes the results. The Figure shows that at higher relative pressure, the amount of gas that entered the pores increased until all pores were occupied at equilibrium. Naturally, the equilibrium was pushed to higher adsorption with higher relative pressure.

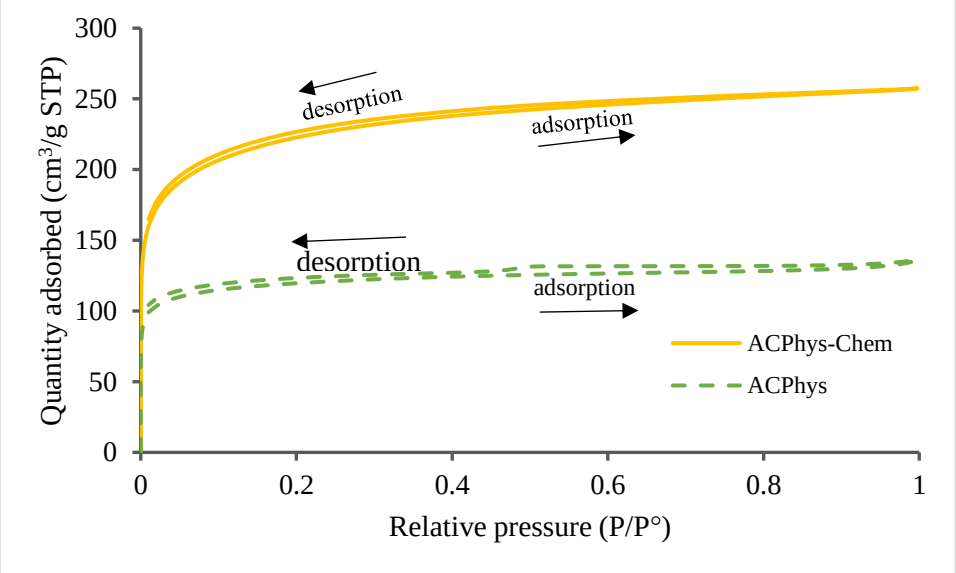

Figure 3. Adsorption isotherms measured for the coffee based ACs. --AC_{Phys} and --$AC_{Phys\text{-}Chem}$.

To understand the effect of pore size distribution, in electrodes on the specific capacitance, BET analyses were performed, Figure 3. The isotherms involved small hysteresis loops from high to low

 doi:10.20944/preprints202410.0924.v1

pressure ranges. This indicated that the electrodes had meso and macro porous structures. According to IUPAC classification, the sample isotherm can be classified as type I, II and IV [40]. Higher nitrogen adsorption, even at very low relative pressures (P/P^o<0.01), for $AC_{Phys\text{-}Chem}$, compared to AC_{Phys} indicated the existence of micropores more in the former than in the latter. The $AC_{Phys\text{-}Chem}$ exhibited higher specific surface area and more micropores than the AC_{Phys}, as described in Table 1. As the minimal pore sizes for $AC_{Phys\text{-}Chem}$ (0.8 nm) and AC_{Phys} (1.8 nm) are larger than the ionic sizes for both electrolyte ions ($K^+_{(hydrated)}$ 0.4 nm, $OH^-_{(hydrated)}$ 0.38 nm), both activated carbons readily adsorb the ions and may behave as supercapacitors. Since the $AC_{Phys\text{-}Chem}$ had more total and micropores than AC_{Phys}, with higher specific surface area, *vide infra*, the former carbon should have higher specific capacitance and lower equivalent series resistance (ERS) than the latter.

The specific surface area was determined by multiple point Brunauer-Emmett-Teller (BET) method in the regions of the isotherms, which are limited by the range of relative pressure P/P^o = 0.0–0.3 as seen in Figure 4. The adsorption volume showed that BET surface areas for AC_{Phys}, and $AC_{Phys\text{-}Chem}$ were 458, 830 m^2/g respectively. The total volume of pores (V_{total}, cm^3/g) was calculated by the number of adsorbed nitrogen at $P/P^o \approx 0.9932$. All results are summarized in Table 1.

Table 1. BET data measured for AC_{Phys} and $AC_{Phys\text{-}Chem.}$

Material	BET based data							
	S_{BET} m^2/g	V_t[b] cm^3/g	$V_{0.5\text{-}2}$[c] mic cm^3/g t-plot	$V_{2\text{-}5}$[e] cm^3/g BJH meso	$V_{>50}$	S mic m^2/g	S Meso m^2/g	APS nm
AC_{Phys}	458	0.2114	0.153	0.23	0.0084	385	73	1.8-3.3
$AC_{Phy\text{-}Chem}$	830	0.41	0.19	0.072	0.148	755	75	0.8-2.7

S_{BET}= BET specific surface area, S_{mic}=Micropore surface area, S_{meso}=Mesopore surface area, S_{macra}=Macropore surface area, V_t= Total pore volumes, V_{mic}=Micropore volume, V_{meso}=Mesopore volume,.

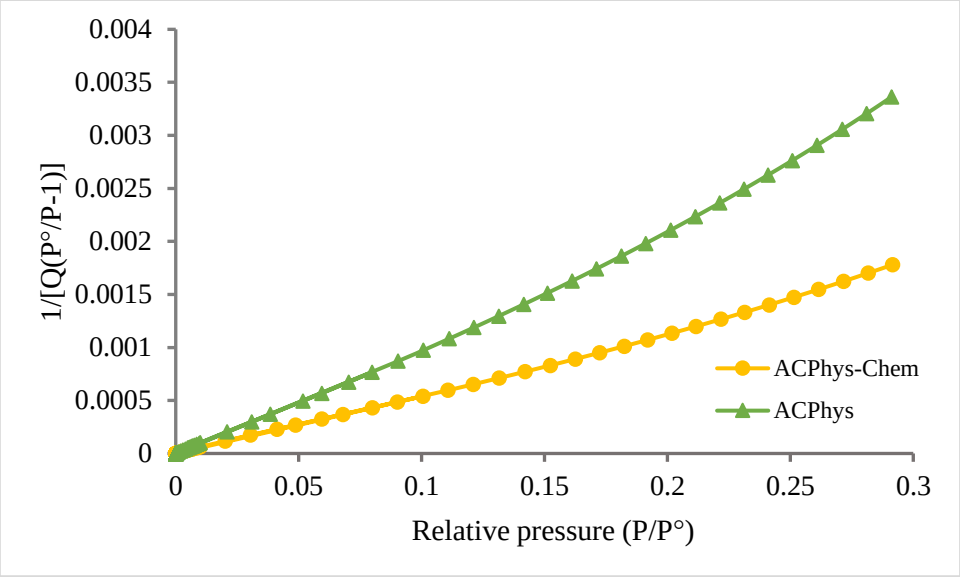

Figure 4. BET plots $1/[Q(P^o/P -1)]$ vs. P/P_0 measured for AC_{Phys} and $AC_{Phys\text{-}Chem.}$

All above results indicated that $AC_{Phys\text{-}Chem}$ high porosity and suitability for super capacitor applications. The increased porosity is due to using the activating agent.

- ***Pore size distribution by the BJH method***

The Brunauer-Joyner-Halenda (BJH) method is very useful to analyze mesopores and macropores in a diameter wide range (17-3000 Å). The pore size distributions in AC_{Phys} and $AC_{Phys\text{-}}$

 doi:10.20944/preprints202410.0924.v1

Chem are summarized in Figure 5. The pore size distributions for the present electrodes were in the micro- , meso- and macropore scales. The Figure shows that for the present electrodes, the domain of pore sizes were centered in the ranges of 1.8-3.3 nm for ACPhys, and 0.8-2.7 nm for ACPhys-Chem. Correlation between BET surface area and pore sizes, with specific capacitance can be understood using Equation (1):

$$C = \varepsilon A/d \quad (1),$$

where C denotes specific capacitance, ε electrolyte-dielectric constant, A specific surface area that is accessible to the ions, and d is spacing between the ions and the electrode pore surface (nm). Based on this Equation, two methods can be followed to improve charge storage for supercapacitors:

- Increasing specific-surface area
- Reducing spacing between ions and electrode surfaces.

The large surface area and high amounts of meso and micro pores together yield high transport of charges leading to high specific capacitance.

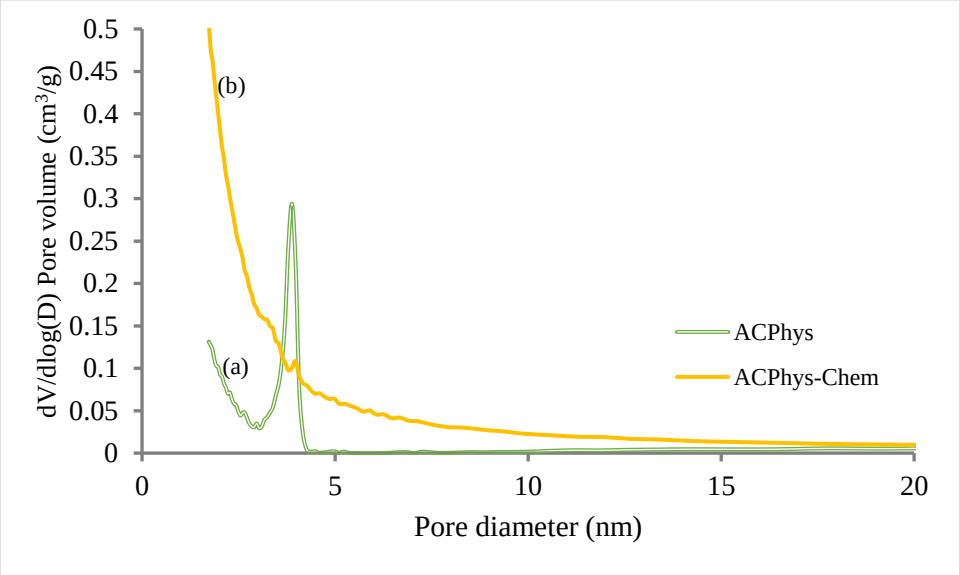

Figure 5. BJH pore size analysis for activated carbons based on BJH method. (a) –ACPhys and (b) – ACPhys-Chem.

The results showed that, for both present ACs, higher adsorbed gas occurred in the smaller pore size. Small pore sizes were more dominant in the ACPhys-Chem, as observed from pore-size distribution (differential pore volume), Figure 5. The observed ACPhys-Chem material peaks were distributed within the pore size range 1.8 – 3.3 nm, with the maximum adsorption at 3.3 nm. Thus, mesopores were dominant in the ACPhys-Chem, with higher adsorption at smaller diameter mesopores. The results justified the high specific capacitance for ACPhys-Chem, as summarized in Table 1.

- ***Pore size distribution by the (HJ) t-plot***

The volume of micropores and the values of micropore surface areas of (S_{micro}, m^2/g) were investigated by the t-Plot Harkins and Jura. The Harkins-Jura t-plot method can analyze micropores with surface areas. The amount of adsorbed N_2, for a given P/P_0 range, is plotted against pore thickness (t). The micropore volumes and surface areas (S_{micro}, m^2/g) were investigated by the t-Plot Harkins and Jura method. The results are summarized in Figure 6 and Table 1. From Figure 6, the present electrodes involved high micro-surface areas of 557 and 385 m^2/g for ACPhys-Chem and ACPhys electrodes, respectively. This justified the high specific capacitance for ACPhys-Chem as described below.

 doi:10.20944/preprints202410.0924.v1

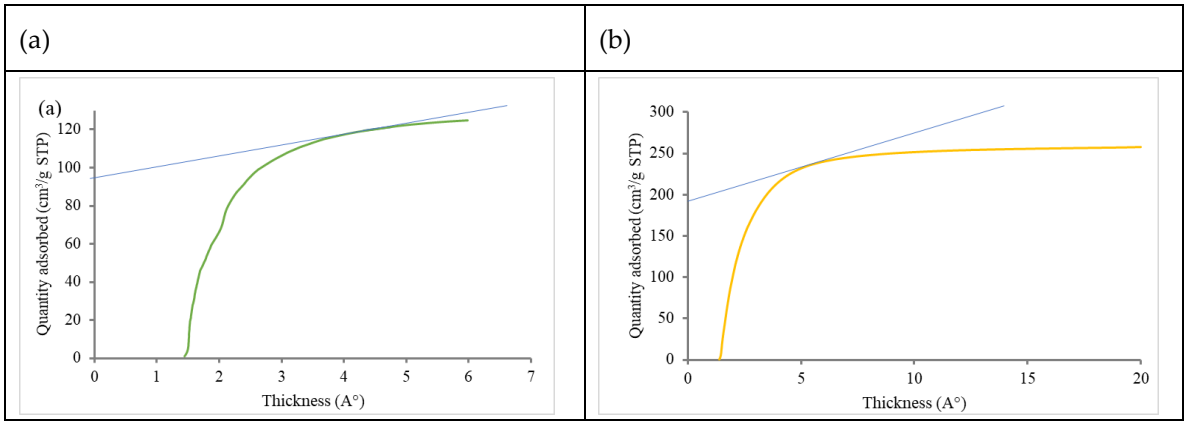

Figure 6. HJ t-plot for N_2 adsorption on (a) --AC_{Phys} and (b) --$AC_{Phys\text{-}Chem}$.

- ***X-Ray patterns***

The XRD pattern is presented in Figure 7. Both AC_{Phys} and $AC_{Phys\text{-}Chem}$ exhibited a reflection at 2ɵ=~24º. The refection is consistent with earlier literature [41]. However, as both materials are amorphous, only broad and low reflections for the (002) signals were observed. The reflection for $AC_{Phys\text{-}Chem}$ was sharper than for AC_{Phys}, which indicates that the former is more crystalline. This means that the former has more carbon content than the latter. Another broad reflection in the range 2ɵ=40-50º can be observed more obviously for $AC_{Phys\text{-}Chem}$ than for AC_{Phys}. The $AC_{Phys\text{-}Chem}$ thus showed more resemblance to earlier chemically activated carbons [42]. The XRD patterns were consistent with the $AC_{Phys\text{-}Chem}$ having higher porosity.

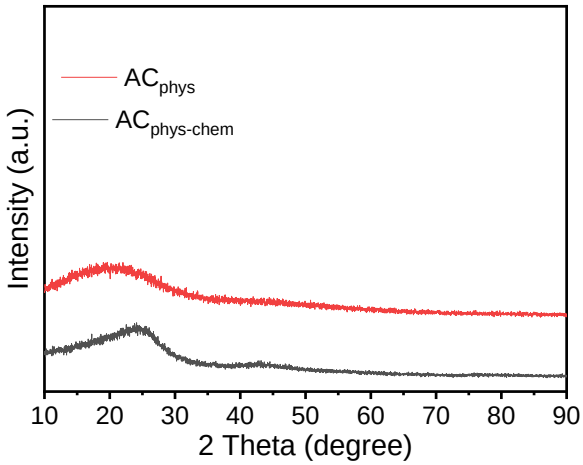

Figure 7. XRD patterns measured for – AC_{Phys} and -- $AC_{Phys\text{-}Chem}$.

- ***Elemental analysis***

For both AC_{Phys} and $AC_{Phys\text{-}Chem}$, elemental analyses were performed by the *EDS*, as described in supplementary Figures S1(a) and (b). The results are summarized in Table 2.

Table 2. Summary of elemental analysis results for (a) $AC_{Phys\text{-}Chem}$ and (b) for AC_{Phys}.

	Element	C	N	O	S	Cl	Fe
a	Atom%	93.3	2.3	3.9	0.1	0.2	$1x10^{-2}$
	Mass%	96.6	0.3		0.1	0.2	$2x10^{-2}$
	Element	C	N	O	S	Cl	Fe
b	Atom%	63.2	1.9	23.7	0.04	1.1	0.04
	Mass%	83.3	4.0		0.1	1.5	0.1

 doi:10.20944/preprints202410.0924.v1

For $AC_{Phys\text{-}Chem}$, the atom percentage for carbon was 93%, while for AC_{phys} it was only 63.20%. So, more carbon appears in $AC_{Phys\text{-}Phem}$, which is a virtue for this material. The EDS results were consistent with the XRD results, in the sense that $AC_{Phys\text{-}Chem}$ material had higher graphitization.

- ***Raman spectra***

Figure 8 below summarizes the Raman spectra for AC_{phys} and $AC_{phys\text{-}chem.}$ The $AC_{Phys\text{-}Chem}$ exhibited higher homogeneity (Figure 8b) than AC_{Phys} (Figure 8a). Both ACs showed two sharp peaks at 1360 cm^{-1} (D peak) and 1590 (G peak). Comparison between the two spectra indicated that D peak intensity (I_D) to the G peak intensity (I_G) is 0.7 for $AC_{Phys\text{-}Chem}$ compared to 0.8 for AC_{Phys}. A lower I_D/I_G ratio means higher graphitization in the AC, as reported in literature [43][44]. Therefore, the $AC_{Phys\text{-}Chem}$ here had more graphitization than the AC_{Phys}. This result corroborates the XRD and EDS results discussed above, in the sense that the former has more C content than the latter.

All in all, the $AC_{Phys\text{-}Chem}$ showed superior characteristics compared to AC_{Phys}. Based on that, the present electrochemical study here was restricted to only $AC_{Phys\text{-}Chem}$ electrode only, in comparison with earlier literature.

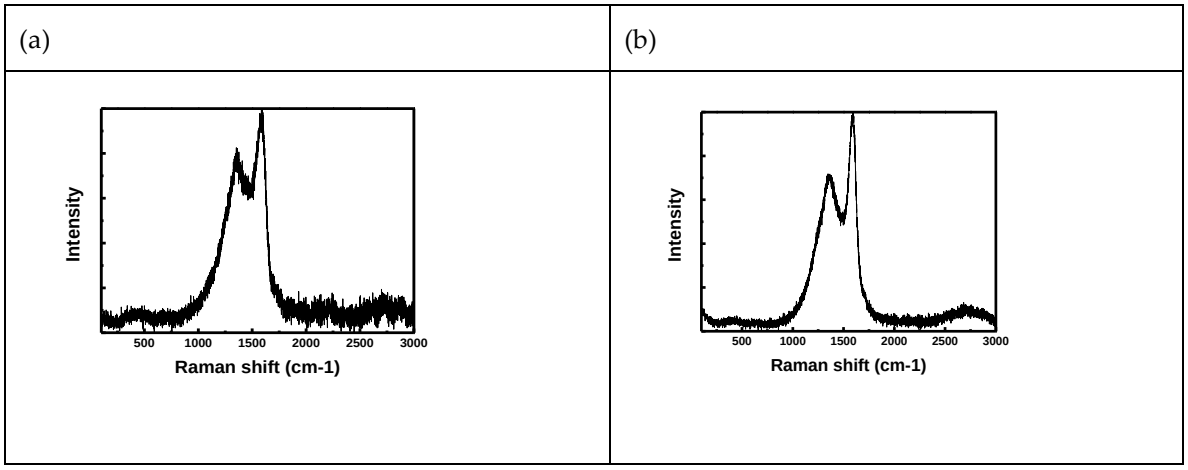

Figure 8. Raman spectra measured for a) AC_{Phys} and b) $AC_{Phys\text{-}Chem}$.

3.2. Supercapacitor Testing

As described above, the $AC_{Phys\text{-}Chem}$ electrode was singled out for further electrochemical study, unless otherwise stated. Cyclic voltammetry (CV), Galvanostatic charge/discharge behaviors (GCD) and electrochemical impedance (EIS) behaviors were investigated for the $AC_{Phys\text{-}Chem}$, using KOH (6.0 M).

- ***Cyclic voltammetry (CV)***

CV is the most fitted method to recognize the capacitive characterization. Cyclic voltammograms were measured in the range of 0.0 to 1.0 V at different scan rates (5, 10, 20, 50 and 100 mV/s) for the $AC_{Phys\text{-}Chem}$ electrode, as shown in Figure 9. Figure 9(a) shows the CVs measured at various scan rates and Figure 9(b) shows CV at low scan rate (5 mV/s) only. At all scan rates, the electrode exhibited symmetrical CV curves. At all scan rate, also, the CV curves exhibited semi-rectangular shapes without any peaks and with high reversible charge-discharge process. The electrode thus behaved as an electronic double layer capacitor (EDLC) [45-49]. The specific capacitance was calculated from the CVs using Equation (2).

$$C_s = \frac{2*(q_a+|q_c|)}{m\Delta V} \quad (2)$$

where C_s is the specific capacitance in F g^{-1}, m is the mass of the active material in g, ΔV is the voltage window in V, q_a and q_c are the anodic and cathodic charges in C, respectively.

The high reversibility for $AC_{Phys\text{-}Chem}$ electrode at various scan rates, and the response (in charging/discharging) were due to high conductivity, as described earlier [50-52]. Based on Figures 9(a) and (b), the specific capacitance values for $AC_{Phys\text{-}Chem}$ were plotted vs. scan rates. Figure 9(c) indicates that specific capacitance decreased at higher scan rate. Table 3 summarizes the results. The

 doi:10.20944/preprints202410.0924.v1

Table shows that the present $AC_{Phys\text{-}Chem}$ electrode was superior to earlier coffee waste-based electrodes in terms of specific capacitance value.

Typically, high specific capacitance is associated with low scan rate. In $AC_{Phys\text{-}Chem}$ the same behaviour was observed. This is due to ions having enough time to penetrate the micropores (with less than 2 nm). At higher scan rates, only larger pores mesopores (2-50 nm) may contribute to capacitance. This is a result of the electrolyte diffusion rate difference in the pores with different sizes. It may also be due to network connections between larger and smaller pores [52-54].

The high specific capacitance of $AC_{Phys\text{-}Chem}$, was partly due to its higher surface area and microporous structure. This increases accessible areas for electrolyte ions storage within the relatively smaller pores. Other factors, such as conductivity, may have influence, as described below.

The increased current density peak with higher scan rate was due to higher ion mobility. This is associated with high concentrations that diffuse in close proximity to electrode surfaces [55, 56].

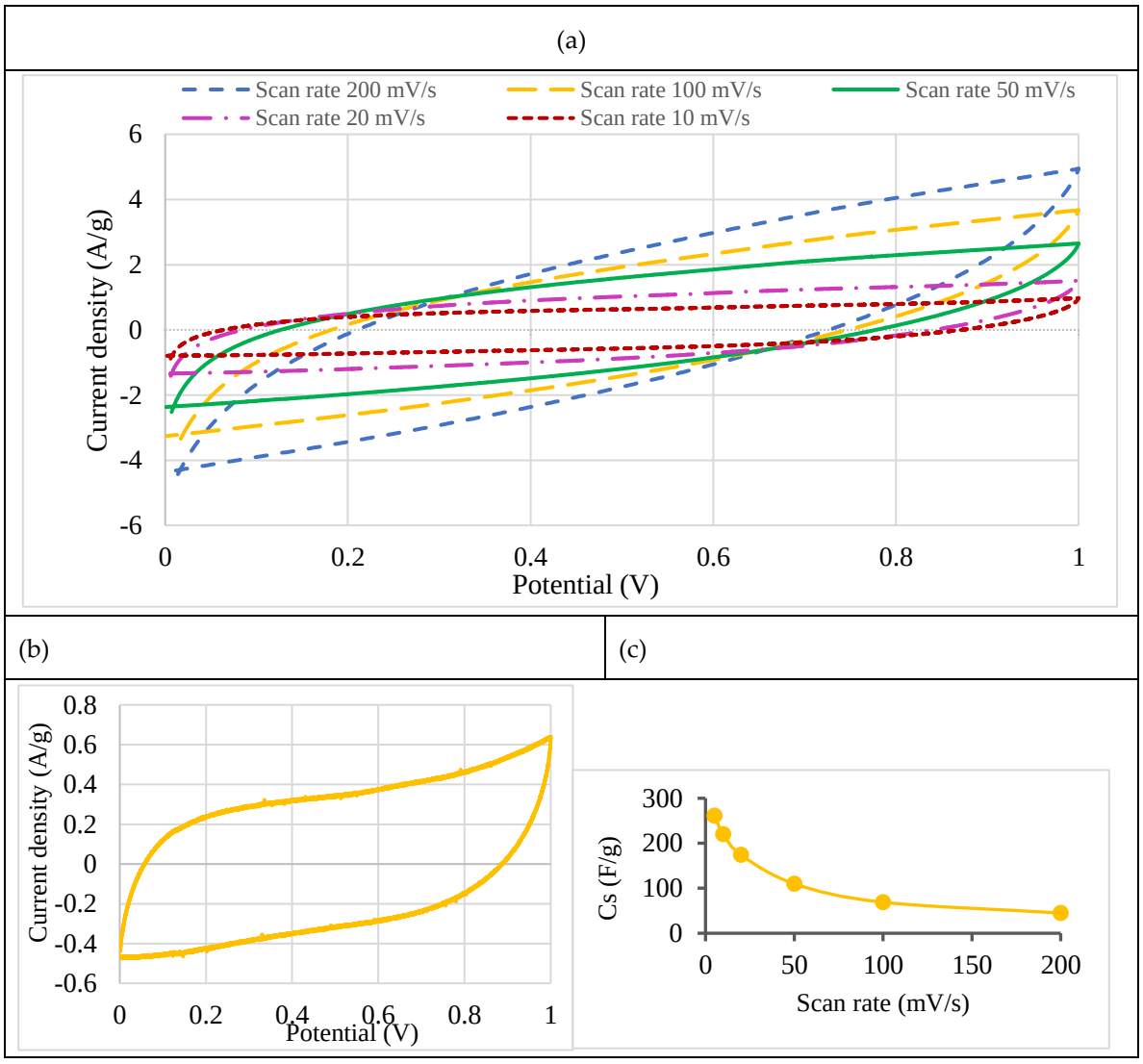

Figure 9. CV studies on $AC_{Phys\text{-}Chem}$ electrode. (a) at various scan rates (b) at scan rate 5 mV/s, (c) scan rate effect on specific capacitance calculated at various.

 doi:10.20944/preprints202410.0924.v1

Table 3. Summary of specific capacitance (C_s) values obtained at various scan rates for $AC_{Phys\text{-}Chem}$ electrode compared to literature.

Scan rate (mV/s)	*Cs* this work (F g^{-1})	Literature C_s (F g^{-1}) for coffee waste-based electrodes
1	--	150 [57]
5	261	109 [33]
10	220	101 [33]
20	174	130 [57] 90 [33]
50	110	100 [57]
100	69	47 [33]
200	45	--

- ***Galvanostatic charge/discharge (GCD)***

The supercapacitor performance can be further tested and verified by GCD method, Figure 10. The $AC_{Phys\text{-}Chem}$ electrode was charged and discharged, galvostatically here, in the potential range (0.0-1.0 V) at various constant discharge current densities of (0.33, 0.67, 1.67, 3.3, 5.0 A g^{-1}). Figure 10(a) summarizes the potential (V) vs. time (s) plots, showing the charge and discharge processes. A potential drop (V_{IR}) was observed in the discharge after the maximum potential value was reached. From Figure 10(a), the potential drops occurred in the discharge processes. The potential drop values were: 0.064, 0.134, 0.297, 0.66 and 0.76 V at the above current density values, respectively. The specific capacitance (C_s) values from the charge discharge curves were estimated using Equation 3 [58], as summarized in Table 4.

$$C_s = {(2 \times I)}/{[(dV/dt) \times M]} \quad (3)$$

where C_s is the specific capacitance, dv/dt is the slope of the linear discharge curve, I is the discharge current in A, and M is the total electrode mass (in g).

The values for equivalent series resistance (ESR), from GCD method, described in Table 4, can be evaluated by Equation (4). The ESR values were within a narrow domain, which confirms the electrode stability at different densities. This is another superior feature for the electrode.

$$ESR = V_{IR}/2I \quad (4)$$

Table 4. Equivalent series resistance values measured at various discharge current values for $AC_{Phys\text{-}Chem}$.

Discharge Current (A)	0.01	0.02	0.05	0.10	0.15
V_{IR} (V)	0.064	0.134	0.297	0.660	0.760
ESR (Ω)	3.20	3.35	3.00	3.30	2.53
Specific Capacitance (F g^{-1})	150	141	92	50	39

It can be seen that each charge and discharge processes is nearly symmetric, which illustrates excellent electrochemical reversibility of the electrode. The small V_{IR} drop in the discharging curves of $AC_{Phys\text{-}Chem}$ implies a small equivalent series resistance, which is essential to power characteristics of supercapacitors. The low V_{IR} drop of $AC_{Phys\text{-}Chem}$ is due to its high conductivity, as achieved by $ZnCl_2$ activation. The specific capacitance of $AC_{Phys\text{-}Chem}$ decreases from 150 F g^{-1} (at current density 0.33 Ag^{-1}) to 39 Fg^{-1} (at 5 Ag^{-1}). The specific capacitance for $AC_{Phys\text{-}Chem}$ decreased with increased current density as shown in Figure 10(b), which common in supercapacitors. This mainly caused by electrolyte ion diffusion limitations.

As the current increases the time needed for charging and discharging processes decreases due to higher ion mobility. This leads to lower C_s, as expected, in congruence with literature [45, 46, 59]. Figure 10(a) shows that as the current density increases, shorter time for charging and discharging is needed. Thus, the voltage drop increases at higher current density, corresponding to the resistance exhibited by the supercapacitor [58, 60].

Preprints.org (www.preprints.org) | NOT PEER-REVIEWED | Posted: 11 October 2024 doi:10.20944/preprints202410.0924.v1

The specific power and specific energy have been calculated using Equations (5) and (6) [61, 62].

$$E = \left[C_s \times (\Delta V_{op})^2\right] / (2 \times 3.6) \quad (5)$$

$$P = E \times 3600 / \Delta t \quad (6)$$

where C_s is specific capacitance (Fg^{-1}) extracted from the discharge curve, ΔV_{op} is operating voltage range (V) defined as $\Delta V_{op} = \Delta V_{appl} - V_{IR}$, ΔV_{appl} (= 1 V) is applied voltage used during charge/discharge process. Δt is discharge time (s) and V_{IR} is voltage drop observed in the discharge plot caused by immediate impact of charge-to-discharge process transition.

Figure 10(c) shows the Ragone plot for electrode. The maximum specific energy is 18.3 Wh/kg at the specific power 360 W/kg at current density 0.33 A/g, while the maximum specific power is 1444 W/kg at specific energy 6.4 Wh/kg at current density 1.66 A/g. These values are higher than most recent literature [33] results for coffee waste electrodes, which showed specific energy 4.78 Wh/kg and specific power 137 W/kg at 1-5 A/g current density. The results confirm the potential value for the present electrode in future application, as it combines high specific energy and specific power together.

The electrode stability on recycling is depicted in Figure 10(d). The plot has been constructed at current density 0.33 A/g for 5,000 cycles, and shows a slight decrease in specific capacitance from 149 to 148 F g^{-1}. The results depict the high electrode stability upon charge-discharge cycling, which is an important feature in supercapacitor technology.

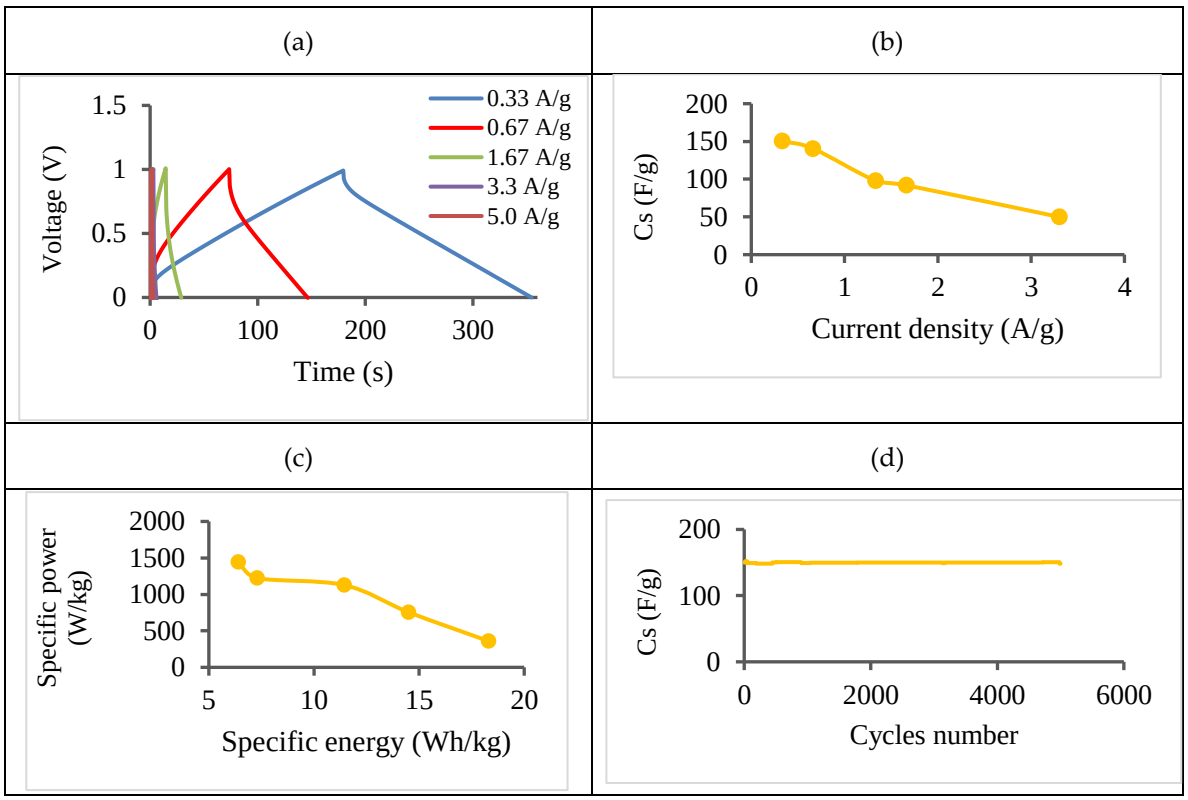

Figure 10. GCD data for $AC_{Phys\text{-}Chem}$ electrode. (a) Charge/discharge at various current densities (b) Values of specific capacitance vs current density, (c) Ragone plot for specific power vs specific energy, (d) Electrode stability with cycling at current density 0.33 A g^{-1}.

- ***Electrochemical impedance spectra (EIS)***

To further confirm the above results, *EIS* was studied, Figure 11. Nyquist plots were constructed for the electrode within the frequency range 0.01 Hz - 10 kHz, Figure 11(a). The *ESR* values indicate looseness inside the supercapacitor. The x-axis intercept, at the higher frequency, represented the combined resistance (R_S= 0.48 Ω) involving electrode material inherent resistance, ionic resistance in electrolyte solution and the contact resistance between the current collector and the electrode. The

 doi:10.20944/preprints202410.0924.v1

semi-circle loop described the electrode conductivity together with its charge-transfer resistance (R_{ct}) [63]. The measured R_{ct} here was 0.2 Ω). Higher electrode conductivity normally indicates smaller semicircle loop. The calculated *ESR* (R_s + R_{CT}) here was 0.6 Ω. At low frequencies, the vertical line describes the electrode capacitive behaviors. In the present electrode, the Nyquist plot showed almost a straight line parallel with the imaginary axis, indicating exactly polarized systems. Deviation from the vertical line, at lower frequencies, to smaller slopes corresponds to higher ionic-diffusion resistance contribution.

The time constant divides between the supercapacitor capacitive and resistive regions. This can be determined by taking the reciprocal of the maximum frequency f_0 as ($t_0 = 1/f_0$). Generally, a low time constant value is a higher-performance indicator, meaning a supercapacitor delivering higher powers in short times. The knee frequency is 0.08 Hz and the time constant is 12.5 s for electrode. Time constant is affected by various factors, including the material conductivity, the electrolyte and the electrode thickness [64]. When the electrode thickness and the electrolyte are kept the same in the supercapacitors, then time constant is influenced only the electrode materials conductivity.

Specific capacitance values, for the supercapacitor, were calculated from impedance analysis using the impedance imaginary component by Equation (7) [60, 65].

$$C_s = 4 \times \left({}^{-1}/_{2\pi f z'' M}\right) \qquad (7)$$

where f is frequency (in Hz), z'' is impedance imaginary component (in Ω), and M is the mass of electrode mass (in g)

Figure 11(b) shows how specific capacitance varies with frequency. The obtained specific capacitance for electrode 179 F g^{-1} at frequency of 0.01 Hz.

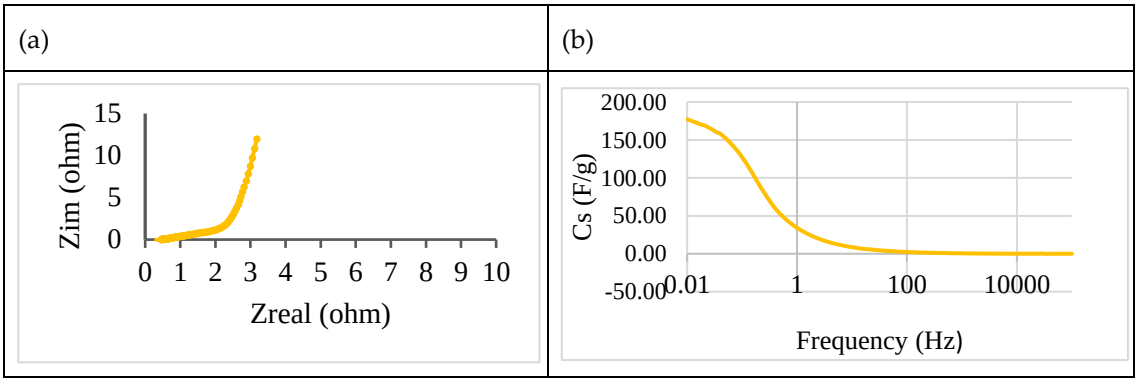

Figure 11. *EIS* data measured for $AC_{Phys\text{-}Chem}$ electrode. (a) Nyquist plot constructed (b) Plot of specific capacitance vs. frequency.

As described above, the specific capacitance for the $AC_{Phys\text{-}Chem}$ was calculated by three methods. The CV study yielded a specific capacitance value 261 F g^{-1}, at scan rate 5 mV/s, that higher than literature values for coffee waste electrodes. The GCD study yielded specific capacitance 150 F g^{-1} at discharge current 0.01 A, and ESR values in the range 2.53-3.2 Ω at discharge currents ranging 0.15 – 0.01 A. The EIS study showed specific capacitance of 179 F g^{-1} at frequency 0.01 Hz with low resistance. All values are superior to earlier reported values, as described above.

All in all, the results indicate that the $AC_{Phys\text{-}Chem}$ electrode exhibited favorable physical characteristics leading to super capacitor performance. As described above, the chemical activating agent improved all characteristics of the activated carbon in many ways. Graphitization and C content were improved. The solid porosity was improved and yielded higher ion uptake. The relative crystallinity was improved, which increased the electrical conductivity within the activated carbon. All these characteristics, enabled the present $AC_{Phys\text{-}Chem}$ electrode to exhibit high specific capacity and output power at the same time. The present electrode here exceeds earlier coffee waste-based electrodes, physically and chemically activated with various materials, both in specific capacitance and in power output density. By combining high supercapacitance and power output together, the present electrode is superior to many electrodes prepared from other biowastes and commercial

 doi:10.20944/preprints202410.0924.v1

carbon. This feature makes the electrode a potential candidate for future commercial supercapacitors. Therefore, it is necessary to examine new chemical activating agents, such as $ZnCl_2$, in producing activated carbons from coffee and other biowastes. Research is active in these laboratories to further improve coffee waste-based ACs by other additional methods.

4. Conclusions

Two activated carbons were prepared from coffee wastes, one by physical method (AC_{Phys}) with no added activators, and the other with $ZnCl_2$ addition ($AC_{Phys\text{-}Chem}$). The latter exhibited super characteristics in terms of specific surface area, porosity, carbon content, graphitization and surface morphology. For these reasons, the $AC_{Phys\text{-}Chem}$ electrode was singled in assessment as a supercapacitor electrode. The new electrode exhibited high specific capacitance values that exceeded literature coffee waste-electrodes. The electrode also exhibited stability with power output values higher than earlier electrodes. With these combined features, the new electrode competes with other reported electrodes produced from other biowastes that showed high performance in literature. Using new types of chemical activators for coffee waste-based electrodes, and using other preparation methods, is recommended in future research.

Supplementary Materials: The following supporting information can be downloaded at the website of this paper posted on Preprints.org.

Author Contributions: S.M.: Investigation (lab experiments and measurements), writing draft manuscript. A.D.: Conceptualization, supervision, validation, writing-review and editing, training, validation. H.N.: Supervision and training, validation, writing-review and editing. S.H.: Validation, writing-review editing. H.L.: Investigation characterization. H.H.: Investigation and characterization. T.W.K.: Investigation and characterization, supervision, validation. H.S.H.: Supervision, writing-review editing, validation. All authors have read and agreed to the published version of the manuscript.

Funding: S.M. acknowledges support from An-Najah National University in the form of "thesis funding policy". T.W.K. acknowledges support from "the National Research Council of Science & Technology (NST) grant by the Korean government (MSIT) (No. CAP20034-200)". No special fund was available for this project.

Data Availability Statement: Data will be available upon request.

Acknowledgments: The results are mainly from S.M. PhD thesis. Help from the technical staff at the University laboratories is acknowledged.

Conflicts of Interest: The authors declare no conflicts of interest.

References

1. H. Huang, X. Wang, Graphene nanoplate-MnO2 composites for supercapacitors: a controllable oxidation approach, Nanoscale, 3 (2011) 3185-3191.
2. Q. Cheng, J. Tang, J. Ma, H. Zhang, N. Shinya, L.-C. Qin, Graphene and nanostructured MnO2 composite electrodes for supercapacitors, Carbon, 49 (2011) 2917-2925.
3. H. Yang, Graphene-based supercapacitor for energy storage applications, in, Thesis, Ohio State University, 2013.
4. Arvinder Singh, Alexander J. Roberts, Robert C. T. Slade and Amreesh Chandra, High electrochemical performance in asymmetric supercapasitor using MWCNT/nickel sulfide composite and graphene nanoplates as electrodes, Journal of materials chemistry A, 2 (2014) 16723-16730. https://doi.org/10.1039/C4TA02870H
5. J. Libich, J. Máca, J. Vondrák, O. Čech, M. Sedlaříková, Supercapacitors: Properties and applications, Journal of energy storage, 17 (2018) 224-227.
6. M. Vangari, T. Pryor, L. Jiang, Supercapacitors: review of materials and fabrication methods, Journal of energy engineering, 139 (2013) 72-79.
7. F. Lufrano, and P. Staiti. Mesoporous carbon materials as electrodes for electrochemical supercapacitors, international journal of electrochemical science, 5 (2010) 903-916. https://doi.org/10.1016/S1452-3981(23)15331-4
8. Mao Lu, Graphene-Based Material for supercapacitor electrode, in, Thesis, National University of Singapore. 2013. https://core.ac.uk/download/pdf/48678913.pdf
9. R. Kötz, M. Carlen, Principles and applications of electrochemical capacitors, Electrochimica Acta, 45 (2000) 2483-2498.

10. Q. Guo, X Zhou, X. Li, S. Chen, A. Seema, A. Greiner and H. Hou Supercapacitors based on hybrid carbon nanofibers containing multiwalled carbon nanotubes, J. Materials Chemistry 19 (2009) 2810-2816. https://doi.org/10.1039/B820170F
11. Meryl D. Stoller and R.S. Ruoff, Best practice methods for determining an electrode material's performance for Ultracapacitors, J. Energy & Environmental Science, 3 (2010) 1294-1301. **https://doi.org/10.1039/C0EE00074D**
12. R. Kotz, M. Carlen, Principles and applications of electrochemical capacitors., J. ElectrochimicaActa, 45 (2000) 2483-249. https://doi.org/10.1016/S0013-4686(00)00354-6
13. R. Farma, M. Deraman , Awitdrus I.A. Talib , R. Omar , J.G. Manjunatha, M.M. Ishak , N.H. Basri and B.N.M. Dolah, Physical and electrochemical properties of supercapacitor electrodes derived from carbon nanotube and biomass carbon, M.M. Int. J. Electrochem. Sci., 8 (2013) 257 - 273. DOI:
14. 10.1016/S1452-3981(23)14018-1
15. W. Li, J. Peng, L. Zhang, K. Yang, H. Xia, S. Zhang, S.-h. Guo, Preparation of activated carbon from coconut shell chars in pilot-scale microwave heating equipment at 60 kW, Waste management, 29 (2009) 756-760.
16. J. Arrebola, A. Caballero, L. Hernán, J. Morales, M. Olivares-Marín, V. Gómez-Serrano, Improving the performance of biomass-derived carbons in Li-ion batteries by controlling the lithium insertion process, Journal of The Electrochemical Society, 157 (2010) A791.
17. A.A. Palanichamy Kalyani, Andre Darchen 2015. Obtaining Activated Carbon from Papaya Seeds for Energy Storage Devices. , International Journal of Engineering Sciences & Research Technology, 4 110-122.
18. L.-b.Z. Wei Li, Jin-hui Peng, Ning Li , Xue-yun Zhu, Preparation Of High Surface Area Activated Carbons From Tobacco Stems With K2CO3 Activation Using Microwave Radiation, Industrial Crops and Products, 27 (2008) 341-347.
19. W.M.A.W. Doud. R. H. Hesas, J.N. Sahu, A. Arami-Niya, The Effects Of A Microwave Heating Method On The Production Of Activated Carbon From Agricultural Waste: A Review., Journal of Analytical and Applied Pyrolysis., 100 (2013) 1-11. https://doi.org/10.1016/j.jaap.2012.12.019
20. J.P. Kunbin Yang, C Srinivasakannan, Libo Zhang, Hongying Xia, Xinhui Duan, Preparation Of High Surface Area Activated Carbon From Coconut Shells Using Microwave Heating., Bioresour Technol, 101 (2010) 6163-6169.
21. J.Y. Hwang, M. Li, M.F. El-Kady, R.B. Kaner, Next-generation activated carbon supercapacitors: a simple step in electrode processing leads to remarkable gains in energy density, Advanced Functional Materials, 27 (2017) 1605745.
22. L. Jiang, J. Yan, L. Hao, R. Xue, G. Sun, B. Yi, High rate performance activated carbons prepared from ginkgo shells for electrochemical supercapacitors, Carbon, 56 (2013) 146-154.
23. P. Hong, X. Liu, X. Zhang, S. Peng, T. Zou, Z. Wang, Y. Yang, R. Zhao, Y. Chen, Y. Wang, Potassium sulphate (K2SO4) activation of chestnut shell to oxygen-enriched porous carbons with enhanced capacitive properties, International Journal of Energy Research, 44 (2020) 5385-5396.
24. L. Cheng, P. Guo, R. Wang, L. Ming, F. Leng, H. Li, X. Zhao, Electrocapacitive properties of supercapacitors based on hierarchical porous carbons from chestnut shell, Colloids and Surfaces A: Physicochemical and Engineering Aspects, 446 (2014) 127-133.
25. L. Wan, X. Li, N. Li, M. Xie, C. Du, Y. Zhang, J. Chen, Multi-heteroatom-doped hierarchical porous carbon derived from chestnut shell with superior performance in supercapacitors, Journal of Alloys and Compounds, 790 (2019) 760-771.
26. N. Czerwinska, C. Giosuè, I. Matos, S. Sabbatini, M.L. Ruello, M. Bernardo, Development of activated carbons derived from wastes: coffee grounds and olive stones as potential porous materials for air depollution, Science of The Total Environment, 914 (2024) 169898.
27. M. Pagett, K.S. Teng, G. Sullivan, W. Zhang, Reusing waste coffee grounds as electrode materials: recent advances and future opportunities, Global Challenges, 7 (2023) 2200093.
28. F. Aouay, A. Attia, L. Dammak, R. Ben Amar, A. Deratani, Activated carbon prepared from waste coffee grounds: Characterization and adsorption properties of dyes, Materials, 17 (2024) 3078.
29. A. AlMarzooqi, H. Almazrouei, H. Alhammadi, Drugs Removal from Wastewater with Activated Carbon from Coffee Waste, Int J Biomed Res Prac, 4 (2024) 1-5.
30. C.-H. Kim, S.-Y. Lee, S.-J. Park, Valorization of waste coffee grounds into microporous carbon materials for CO 2 adsorption, Green Chemistry, 26 (2024) 1901-1909.
31. K. Pandey, H.K. Jeong, Coffee waste-derived porous carbon based flexible supercapacitors, Chemical Physics Letters, 809 (2022) 140173.
32. Y.-H. Chiu, L.-Y. Lin, Effect of activating agents for producing activated carbon using a facile one-step synthesis with waste coffee grounds for symmetric supercapacitors, Journal of the taiwan institute of chemical engineers, 101 (2019) 177-185.

33. M. Biegun, A. Dymerska, X. Chen, E. Mijowska, Study of the active carbon from used coffee grounds as the active material for a high-temperature stable supercapacitor with ionic-liquid electrolyte, Materials, 13 (2020) 3919.
34. O. Khadka, U. Lawaju, S. Koju, R.C. Rai, M.L. Nakarmi, P. Joshi, Activated carbon derived from coffee waste as supercapacitor electrode material, Scientific World, 17 (2024) 19-26.
35. J.M. Davidraj, C.I. Sathish, M.R. Benzigar, Z. Li, X. Zhang, R. Bahadur, K. Ramadass, G. Singh, J. Yi, P. Kumar, Recent advances in food waste-derived nanoporous carbon for energy storage, Science and Technology of Advanced Materials, (2024) 2357062.
36. T.E. Rufford, D. Hulicova-Jurcakova, Z. Zhu, G.Q. Lu, Nanoporous carbon electrode from waste coffee beans for high performance supercapacitors, Electrochemistry Communications, 10 (2008) 1594-1597.
37. A. Zyoud, H.N. Nassar, A. El-Hamouz, H.S. Hilal, Solid olive waste in environmental cleanup: enhanced nitrite ion removal by ZnCl2-activated carbon, Journal of environmental management, 152 (2015) 27-35.
38. T.E. Rufford, D. Hulicova-Jurcakova, E. Fiset, Z. Zhu, G.Q. Lu, Double-layer capacitance of waste coffee ground activated carbons in an organic electrolyte, Electrochemistry Communications, 11 (2009) 974-977.
39. P.T. Williams, A.R. Reed, Development of activated carbon pore structure via physical and chemical activation of biomass fibre waste, Biomass and bioenergy, 30 (2006) 144-152.
40. K. Le Van, T. Luong Thi Thu, Preparation of Pore-Size Controllable Activated Carbon from Rice Husk Using Dual Activating Agent and Its Application in Supercapacitor, Journal of Chemistry, 2019 (2019) 4329609.
41. S. Lowell, J.E. Shields, M.A. Thomas, M. Thommes, Characterization of porous solids and powders: surface area, pore size and density, book, Springer Science & Business Media, 2012. pp. 1-4. DOI 10.1007/978-1-4020-2303-3.
42. R. Rajbhandari, L.K. Shrestha, R.R. Pradhananga, Nanoporous activated carbon derived from Lapsi (Choerospondias Axillaris) seed stone for the removal of arsenic from water, Journal of nanoscience and nanotechnology, 12 (2012) 7002-7009.
43. X.-Y. Liu, M. Huang, H.-L. Ma, Z.-Q. Zhang, J.-M. Gao, Y.-L. Zhu, X.-J. Han, X.-Y. Guo, Preparation of a carbon-based solid acid catalyst by sulfonating activated carbon in a chemical reduction process, Molecules, 15 (2010) 7188-7196.
44. Y. Liu, X. Liu, W. Dong, L. Zhang, Q. Kong, W. Wang, Efficient adsorption of sulfamethazine onto modified activated carbon: a plausible adsorption mechanism, Scientific reports, 7 (2017) 12437.
45. G.K. Gupta, P. Sagar, S.K. Pandey, M. Srivastava, A. Singh, J. Singh, A. Srivastava, S. Srivastava, A. Srivastava, In situ fabrication of activated carbon from a bio-waste desmostachya bipinnata for the improved supercapacitor performance, Nanoscale research letters, 16 (2021) 85. https://doi.org/10.1186/s11671-021-03545-8
46. A. Daraghmeh, S. Hussain, L. Servera, E. Xuriguera, M. Blanes, F. Ramos, A. Cornet, A. Cirera, Flexible supercapacitors based on low-cost tape casting of high dense carbon nanofibers, Materials Research Express, 4 (2017) 025007.
47. Q. Ke, J. Wang, Graphene-Based Materials For Supercapacitor Electrodes, J. Mathematics, 2 (2016) 37-54. https://doi.org/10.1016/j.jmat.2016.01.001
48. A. Singh, A.J. Roberts, R.C. Slade, A. Chandra, High electrochemical performance in asymmetric supercapacitors using MWCNT/nickel sulfide composite and graphene nanoplatelets as electrodes, Journal of Materials Chemistry A, 2 (2014) 16723-16730.
49. S.Y. Kim, Y.J. Noh, J. Yu, Thermal conductivity of graphene nanoplatelets filled composites fabricated by solvent-free processing for the excellent filler dispersion and a theoretical approach for the composites containing the geometrized fillers, Composites Part A: Applied Science and Manufacturing, 69 (2015) 219-225.
50. S. Jarrar, S. Hussain, A.U. Haq, G. Bhattacharya, I. Saadeddin, L. Servera, J. Ruiz, A. Janem, A. Daraghmeh, Binder-free all-carbon composite supercapacitors, Nanotechnology, 35 (2024) 305708.
51. S. Prabaharan, R. Vimala, Z. Zainal, Nanostructured mesoporous carbon as electrodes for supercapacitors, Journal of Power Sources, 161 (2006) 730-736.
52. D. Saha, Y. Li, Z. Bi, J. Chen, J.K. Keum, D.K. Hensley, H.A. Grappe, H.M. Meyer III, S. Dai, M.P. Paranthaman, Studies on supercapacitor electrode material from activated lignin-derived mesoporous carbon, Langmuir, 30 (2014) 900-910.
53. E. Frackowiak, F. Beguin, Carbon materials for the electrochemical storage of energy in capacitors, Carbon, 39 (2001) 937-950.
54. C.-S. Lim, K. Teoh, C.-W. Liew, S. Ramesh, Electric double layer capacitor based on activated carbon electrode and biodegradable composite polymer electrolyte, Ionics, 20 (2014) 251-258.
55. S.K. Meher, P. Justin, G. Ranga Rao, Microwave-mediated synthesis for improved morphology and pseudocapacitance performance of nickel oxide, ACS applied materials & interfaces, 3 (2011) 2063-2073.
56. J.W. Graydon, M. Panjehshahi, D.W. Kirk, Charge redistribution and ionic mobility in the micropores of supercapacitors, Journal of Power Sources, 245 (2014) 822-829.

 doi:10.20944/preprints202410.0924.v1

57. R.A.P. Jayawickramage, J.P. Ferraris, High performance supercapacitors using lignin based electrospun carbon nanofiber electrodes in ionic liquid electrolytes, Nanotechnology, 30 (2019) 155402.
58. J. Choi, C. Zequine, S. Bhoyate, W. Lin, X. Li, P. Kahol, R. Gupta, Waste coffee management: deriving high-performance supercapacitors using nitrogen-doped coffee-derived carbon, C, 5 (2019) 44.
59. R. Farma, M. Deraman, I. Talib, R. Omar, J. Manjunatha, M. Ishak, N. Basri, B. Dolah, Physical and electrochemical properties of supercapacitor electrodes derived from carbon nanotube and biomass carbon, International Journal of Electrochemical Science, 8 (2013) 257-273.
60. Sabreen Jarrar, Carbon Nanofibers/Graphene Nanoplateletes Composite as Supercapacitor Electrode Using KOH Aqueous Electrolyte, in, Thesis, An-Najah National University, 2020.
61. A. Daraghmeh, S. Hussain, L. Servera, E. Xuriguera, A. Cornet, A. Cirera, Impact of binder concentration and pressure on performance of symmetric CNFs based supercapacitors, Electrochimica Acta, 245 (2017) 531-538.
62. Y. Zhou, P. Jin, Y. Zhou, Y. Zhu, High-performance symmetric supercapacitors based on carbon nanotube/graphite nanofiber nanocomposites, Scientific reports, 8 (2018) 9005.
63. V. Ganesh, S. Pitchumani, V. Lakshminarayanan, New symmetric and asymmetric supercapacitors based on high surface area porous nickel and activated carbon, Journal of Power Sources, 158 (2006) 1523-1532.
64. Y. Gong, D. Li, Q. Fu, C. Pan, Influence of graphene microstructures on electrochemical performance for supercapacitors, Progress in Natural Science: Materials International, 25 (2015) 379-385.
65. C. Schütter, C. Ramirez-Castro, M. Oljaca, S. Passerini, M. Winter, A. Balducci, Activated carbon, carbon blacks and graphene based nanoplatelets as active materials for electrochemical double layer capacitors: a comparative study, Journal of the Electrochemical Society, 162 (2014) A44.
66. E. Calvo, F. Lufrano, P. Staiti, A. Brigandì, A. Arenillas, J. Menéndez, Optimizing the electrochemical performance of aqueous symmetric supercapacitors based on an activated carbon xerogel, Journal of Power Sources, 241 (2013) 776-782.